Sensors and Actuators B 195 (2014) 473–477

Contents lists available at ScienceDirect

Sensors and Actuators B: Chemical

journal homepage: www.elsevier.com/locate/snb

Optical phase-shift dynamics in surface-modified transparent polymers: Application of wavefront distortion analysis to refractive index (RI)-based sensor development

Donald M. Snyder*

Department of Chemistry, Eastern Michigan University, Ypsilanti 48197, MI, USA

ARTICLE INFO

Article history:
Received 31 August 2013
Received in revised form 15 January 2014
Accepted 17 January 2014
Available online 30 January 2014

Keywords:
Shack–Hartmann interferometer
Refractive index sensor
Wavefront image
Phase sensitive detector
Differential phase shift

ABSTRACT

Optical sensors which are based on slight changes in refractive index (RI) resulting from interaction of an optical substrate with some target species utilize a variety of techniques to quantify the RI modification. Detection schemes based on light propagation within optical fibers measure RI changes by transmission efficiency and/or interferometric techniques. Ellipsometry measures changes in surface RI through amplitude and phase changes for the p- and s- components which alter the angle of reflection for polarized light. An alternate method of relating RI variation to surface adsorption in transparent polymers has been explored using a wavefront sensor of the Shack–Hartmann type. The basic concept has been demonstrated by passing a collimated laser beam through a thin film of polystyrene on glass and analyzing the transmitted wavefront for optical phase-shift of the film relative to the glass in the presence of volatile organic compounds. Changes in magnitude of the overall distortion could be related both to the concentration of the vapor and the solvent/polymer solubility parameter match.

1. Introduction

The majority of spectroscopic techniques utilized in chemical analysis is fundamentally based on absorption of light, where the frequency/wavelength of the absorbance is a function of the differences between quantized energy states. These states are related to some structural feature of the compound, such as covalent bond vibrations (IR spectroscopy), π-bonding conjugation (UV spectroscopy), molecular rotation (microwave spectroscopy), and C&H connectivity effects on local magnetic environment (NMR spectroscopy), among other techniques. Spectroscopy thus depends on the use of intensity-sensitive detectors to quantify variable absorbance. While transparent materials do not absorb visible light, they do induce an optical phase shift in the transmitted light to a degree dependent on sample thickness and refractive index. Optical sensors which are based on detection of the slight changes in refractive index (RI) due to interaction of an optical substrate with some target species utilize a variety of techniques to quantify the RI modification. Early detection schemes were based primarily on light propagation within single-mode optical fibres, where RI changes on the fibre surface can be measured by evanescent-wave induced loss of transmission efficiency, or on planar Mach–Zehnder interferometers where differential phase-shifts between beam paths can also attenuate the transmission intensity [1]. The development of microstructured optical fibres (MOFs), also known as photonic crystal fibres (PCFs) or photonic bandgap fibres (PBFs) has allowed increased evanescent-wave interaction by penetration of the target species through the air channels in the core/cladding region [2]. Coupling such PCFs with standard single-mode fibres in a Mach–Zehnder configuration gave a gas sensor with refractive index resolution of approximately 4×10^{-7} [3]. Long-period-gratings (LPG) in both single-mode solid fibers and photonic bandgap crystal fibers have also been investigated for measurement of very small changes in refractive index [4]. LPG-based refractive index optical biosensors [5,6] and gas sensors [7] have been described.

As a stand-off, reflective technique with relatively simple optics, ellipsometry has also been extensively studied for biosensor applications [8–10]. Ellipsometry measures changes in polarization as light reflects from a material surface, with the measured response dependent on optical properties such as RI, and sample thickness. When linearly-polarized light is used, the reflected light undergoes amplitude and phase changes for both the p- and s- components and these changes alter the polarization angle. For biosensor applications the reflective surface is coated with a biological material with specific binding behavior toward some particular molecule and changes in the angle of reflected polarization correlated with target species concentration.

* Tel.: +1 734 487 1429.
E-mail address: dsnyder@emich.edu

0925-4005/$ – see front matter © 2014 Elsevier B.V. All rights reserved.
http://dx.doi.org/10.1016/j.snb.2014.01.057

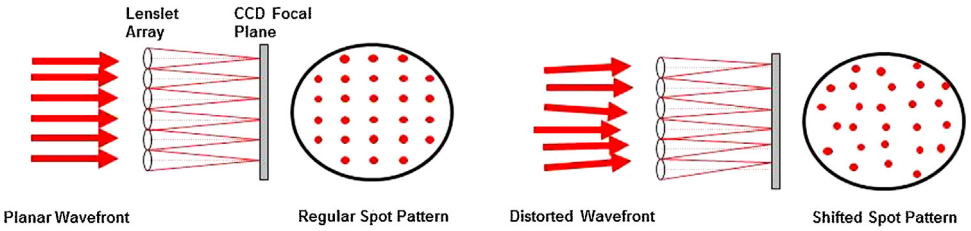

Fig. 1. Operation of a Shack–Hartmann device showing spot pattern changes for planar vs. distorted wavefronts.

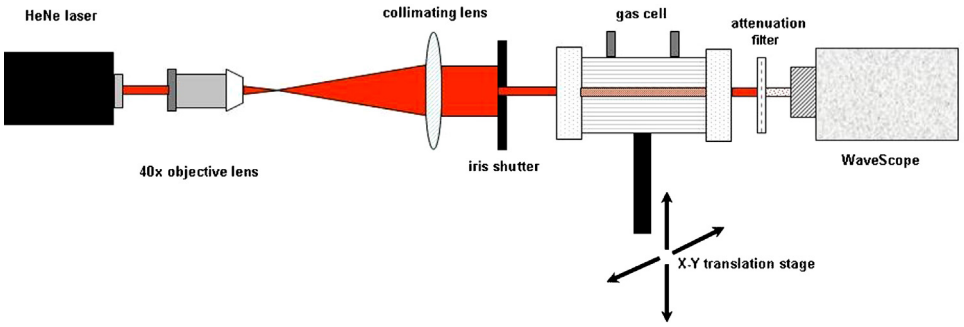

Fig. 2. Configuration of wavefront distortion analysis equipment.

An alternate method of utilizing slight variations in refractive index for quantifying changes in optical behavior lies in transmission of light through transparent materials. When the transparent solid has a non-uniform refractive index, differential phase retardation related to sample inhomogeneity results in a distorted wave front for the transmitted beam. This phase distortion may be mapped by a single-beam interferometer of the Shack–Hartmann type [11–13], which operates by dividing the aberrated wave front into multiple sub-apertures by a grid of microlens ("lenslets"). The spot pattern from the microlens on a CCD focal plane can be analyzed to quantify both the degree and direction of the localized wavefront tilt (see Fig. 1). While phase-sensitive detectors are the fundamental basis for optical wavefront analysis in such diverse fields as laser eye surgery [14] and telescope image enhancement [15], application of the general concept to chemical analysis has been almost completely unexplored. Survey of the literature shows only a few examples of Shack–Hartmann wavefront analysis for optical study of material properties, and these relate primarily to examining laser-induced thermal distortion effects [16–18]. Research at the EMU Laser Physics Laboratory has successfully utilized a S-H wavefront analyzer in development of a novel optical method for monitoring the degree of fusion of PVC plastisols [19]. Continuing work aimed at design of novel optical sensors has now shown that changes in refractive index related to absorption of organic vapors by a transparent polymer film result in changes in the transmitted wavefront distortion pattern that can be correlated to both vapor concentration and solubility parameters.

2. Experimental

2.1. Materials

All chemicals were purchased from Aldrich Chemical Company. Ethyl acetate, hexane, anhydrous ethanol, and all other solvents were reagent grade and used without further purification. The polystyrene (PS) was a 280,000 M_W with T_g = 100 °C.

2.2. Equipment

The Shack–Hartmann instrument used in this study was a WFS-01 WaveScope wavefront sensor from Adaptive Optics Associates, Cambridge, MA with a main aperture of 20 mm. The 0300S lenslet module with a 100 × 100 grid of square lenses of 300 micron pitch (~10–11 lens per mm^2) and an EFL (effective focal length) = 15.8 mm was used for wavefront imaging. With a 6 mm diameter beam spot, the 0300S module yielded ~315 data points per image. A randomly polarized JDS Uniphase Model 1508 0.5 mW, 633 nm HeNe laser was the beam source. Lens, attenuators, mounts,

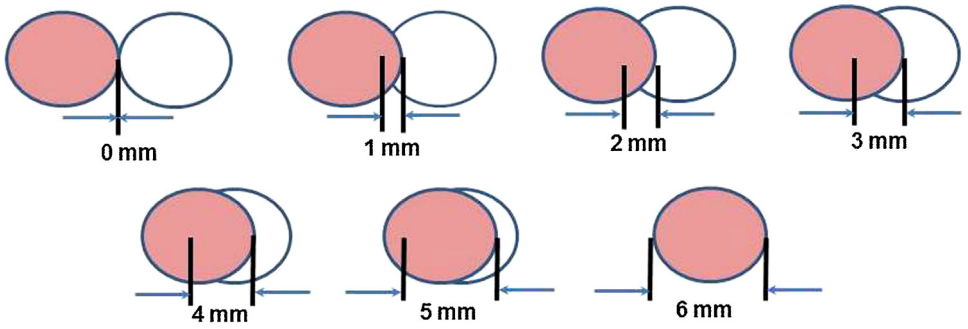

Fig. 3. Beam-film spot overlap settings for baseline RMS values.

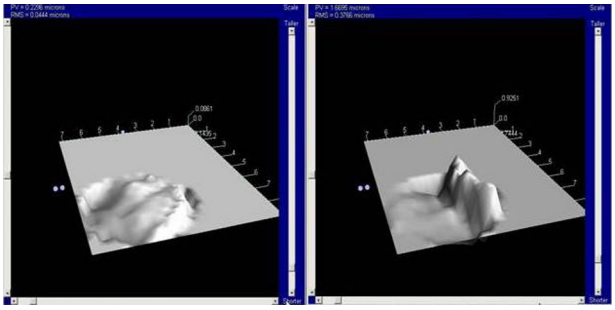

Fig. 4. Baseline wavefront images: 0 mm (left) and 3 mm (right) radial overlap.

and other standard optical bench items were from Newport Corporation, Irvine, CA. The gas cell was a Beta 5-CM unit from Buck Scientific, Norwalk, CT, fitted with Model 10BW40-30 laser-grade parallel windows of BK7 optical glass. The internal volume of the cell was calculated as 12.2 cm^3. The PS film spot was prepared by deposition of a drop of 10 wt% solution of PS in 1:1 MEK/toluene on the surface of a BK7 glass optical blank followed by slow evaporation. After 72 h, the PS sample was annealed at 75–80 °C for 12 h to give a circular film spot which was visually (microscope examination) smooth and regular, 6 mm in diameter with a thickness of approximately 40 micron.

2.3. General measurement procedure

The optical train for the wavefront distortion apparatus is shown in Fig. 2. The 0.48 mm output beam from the HeNe laser is expanded to a collimated beam approximately 20 mm in diameter. An adjustable iris passes only the center of the beam stopped down to a 6 mm diameter, which then passes through the gas cell with the PS film sample on the interior face of one of the windows. The gas cell is mounted on a micrometer-driven X-Y translation stage for adjusting the degree of overlap between the PS film spot and the stationary beam. The WaveScope has a 6-axis adjustable mount for maintaining laser beam alignment parallel with the optical axis. Overall distortion of the beam wavefront was quantified by the root-mean-square (RMS) deviation of spots from their grid centroids. Translation of the gas cell across the stationary beam path adjusted the degree of coincident area between the polystyrene film spot and the laser based on the mm of radial overlap, as shown in Fig. 3. At each overlap setting, the total wavefront distortion was quantified by the image RMS values. After establishing the solvent-free baseline image RMS value, a specific microliter volume of the solvent of interest was injected into the gas cell, which evaporated to give corresponding changes in the wavefront distortion value as a function of the PS film adsorption response. After data acquisition, the cell was flushed with dry N_2 for a minimum of 60 min to remove the organic vapor and return the PS film surface to initial conditions, as evidenced by the constant post-flush RMS baseline monitored prior to each run. The term "baseline RMS value" thus always indicates data acquired in the absence of solvent vapor.

3. Results

3.1. Wavefront distortion as a function of beam/film spot overlap

It was initially hypothesized that the additional phase-retarding effect of the PS film vs. the phase shift of that portion of the laser beam passing only through the glass would result in a distorted wavefront for the transmitted beam, with magnitude and local tilt-patterns related to the degree of overlap between the beam and the film spot. Fig. 4 illustrates the wavefront images for the all-glass baseline (0 mm overlap) vs. the baseline with 3 mm radial overlap of the PS film spot. Since the surface profile at the film edge formed the maximum thickness gradient, it was presumed that the film spot perimeter would be the largest contributor to the total wavefront distortion. As shown in Table 1, increasing the area overlap brought more of the spot perimeter into the image area and did increase the baseline RMS up to the point at which the beam spot and film area were completely coincident. With complete beam/film spot overlap, the total distortion is dominated by the relatively flat area of the film surface and overall RMS thus decreases.

Table 1
Summary of baseline RMS values at specific beam/film spot overlap settings.

Radial overlap (mm)	Area overlap (%)	Baseline RMS value
0	0	0.0163
1	8	0.0220
2	22	0.1484
3	39	0.3273
4	58	0.5110
5	79	0.6378
6	100	0.3660

3.2. RMS variation as a function of vapor concentration

With the gas cell set for 3 mm of radial overlap for all runs, the relationship between wavefront distortion and vapor concentration was studied by monitoring the image RMS value while a measured volume of solvent added to the cell evaporated within. The solubility parameter for polystyrene is usually quoted as 9.10 [20], so a solvent with matching solubility parameter was chosen in order to maximize the probability of rapid surface adsorption and resulting change in the wavefront distortion. Ethyl acetate was used because of its matching solubility parameter of 9.10 and its sufficiently low boiling point (77 °C) to insure complete evaporation of sample volumes <60 μL within 60–90 s at room temperature. Fig. 5 shows that over four separate runs injecting volumes of ethyl acetate of 5, 10, 20, and 30 μL respectively, in each case the initially-steady baseline increased to a maximum value proportional to the liquid volume injected, followed by a slow drift back down toward the baseline. If the run is repeated with the PS film moved completely out of the beam path, there is no significant effect from the solvent vapor on the all-glass RMS value.

3.3. RMS variation as a function of solvent structure

In order to determine if the magnitude of the RMS response for the polystyrene film also varied with solvent structure, multiple

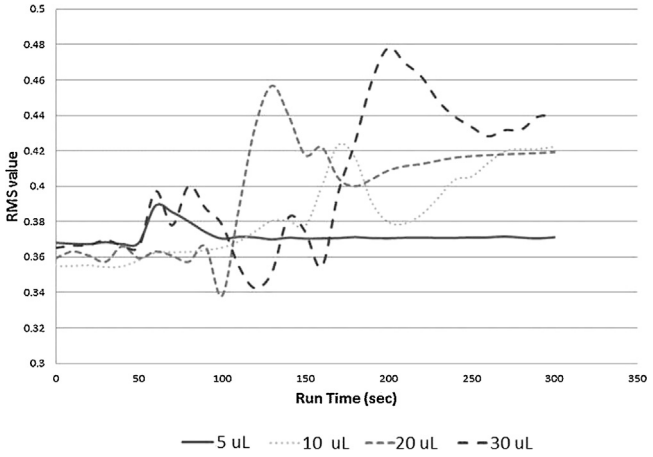

Fig. 5. RMS values vs. time after addition of 5, 10, 20, and 30 μL volumes of ethyl acetate in separate runs.

Table 2
Variation in RMS signal response with solvent structure at equivalent vapor concentrations.

Solvent	Solubility parameter (δ)	$\delta_{PS} - \delta_{solvent}$	(%) RMS change
Ethylacetate	9.10	0	25.2
THF	9.52	0.42	21.9
Acetone	9.77	0.67	19.7
Cyclohexane	8.18	0.92	18.0
Hexane	7.24	1.86	14.1
2-Propanol	11.50	2.40	12.0
CH_3CN	11.90	2.80	8.6
Ethanol	12.92	3.82	4.9

trials were run using a series of different solvents which had volumes for each calculated to give the same molar vapor concentration as the 20 μL aliquot of ethyl acetate. Solvents shown in Table 2 were also chosen to have comparable volatilities to ensure complete vaporization within the usual run-time.

4. Discussion

The initial hypothesis that a single-beam interferometer of the Shack–Hartmann type could be used to quantify small changes in refractive index related to specific chemical events was tested by determining changes in the wavefront image for a laser beam transmitted through a polymer film under varying conditions. With a fixed configuration of the optical train, wavefront images were established in the absence of organic vapors to determine baseline RMS values as a function of the degree of laser beam/film spot overlap. As anticipated, the total wavefront distortion, expressed by the image RMS value, generally increased with increasing overlap.

Based on this study, the set-up with 3 mm of overlap was selected as part of the standard instrument configuration. Table 1 shows that the 3 mm beam/film spot overlap setting gave a baseline RMS of 0.3273. Since all of the baseline RMS values in Table 1 were subject to a small, relatively-constant degree of random deviation, the greater overlap settings showed proportionally more stable baselines. However, on the assumption that the changes in RMS values due to solvent adsorption would also be relatively constant, the calculated %RMS change would be expected to be smaller for the larger baselines. The intermediate setting of 3 mm was thus selected in an effort to optimize baseline stability while also maximizing the %RMS change for all subsequent testing of RMS change with solvent concentration and/or solvent structure.

It was clearly seen that as the concentration of ethyl acetate vapor was increased, the wavefront RMS value increased correspondingly to a maximum value proportional to the liquid volume injected, followed by a slow drift back down toward the baseline. Whether this behavior is due directly to small changes in refractive index of the solvated polymer or a slight change in film thickness related to simple mechanical swelling, or a combination of both effects could not be reliably determined in this study. It has been hypothesized that the initial rapid increase in wavefront RMS value to a maximum followed by a slow decline is most likely due to competing kinetic aspects of the adsorption process. An initial rapid up-take to give a solvent-rich surface layer, followed by a slower process of Fickian diffusion of the solvent molecules deeper into polymer would result in a more diluted region of refractive index change, further complicated by effects of swelling on surface topography that could also influence wavefront transmission and account for slow changes in the distortion. In order to compare RMS changes between runs on a more consistent basis, the differences between baseline and curve maxima were divided by the baseline for each run to express them as a % of the baseline. The use of the curve maxima as the basis for calculation of the %RMS change values rather than the average of all the RMS data points after solvent injection was for consistency of results. Each run had a single, well-defined maximum but times to reach that point varied and not all the runs were tracked to the same time afterwards, as the shape of the graphical plot was not considered critical. As shown by Fig. 6, when the "% RMS Change" for the 4 curves of Fig. 5 were plotted vs. the calculated molar concentration of ethyl acetate vapor in the gas cell for each, a reasonably linear proportionality was observed over the concentration range tested. The error bars for Fig. 6 were routine standard deviation calculations for triplicate runs at each ethyl acetate concentration.

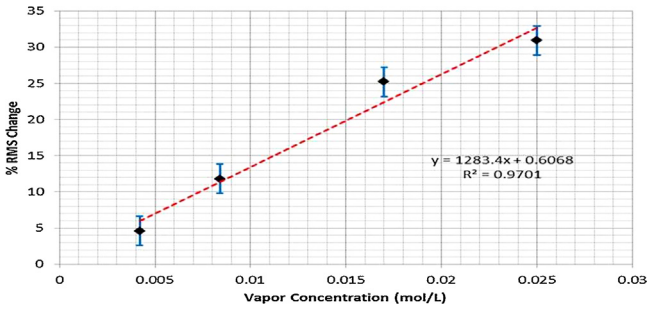

Fig. 6. %RMS change vs. calculated gas concentration [M] for ethyl acetate.

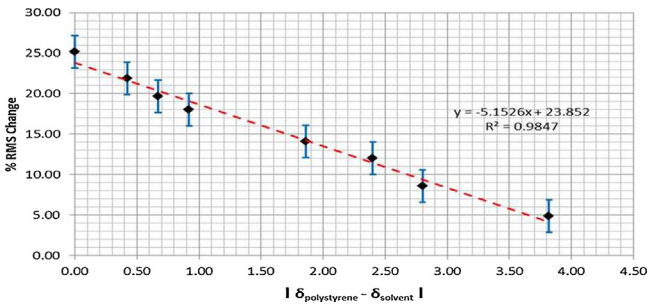

Fig. 7. Summary of %RMS change at equivalent vapor concentrations as a function of $\Delta\delta$.

Since the degree of surface adsorption should also be related to the similarity between solubility parameters of the polymer and the solvent vapor, it was expected that as the difference increased, wavefront RMS values should decrease and vice-versa. A series of organic liquids of similar volatility but different solubility parameters were tested at equivalent concentrations to determine how RMS changes were related to molecular structure and polarity characteristics. Results from Table 2 clearly showed that as the solubility parameters for the volatile solvents became increasingly mismatched from polystyrene, the RMS signal response for the PS film decreased. A plot of the RMS values versus difference in solubility parameters shown as Fig. 7 indicates a closely linear relationship between these parameters.

5. Conclusions

Surface adsorption of a solvent vapor by a thin film of polymer such as polystyrene, has been shown to give a readily measureable change in the optical phase shift of a laser beam transmitted through the film. If the transparent solid has a non-uniform refractive index due to variable composition, or shape, or a combination of both factors, differential phase retardation related to sample inhomogeneity will result in a distorted wavefront for the transmitted beam. A single-beam interferometer of the Shack–Hartmann type can be used to quantify changes in wavefront distortion through various measurements on the S-H wavefront image. In

this study, a simple numerical value for overall distortion of the wavefront was assigned on the basis of the root-mean-square (RMS) deviation of wavefront image spots from their grid centroids. Using the RMS values, it has been demonstrated that the change in wavefront distortion associated with surface adsorption of organic vapors into the polymer surface can be directly related to the airborne concentration of that vapor. This detection mechanism offers potential applications in development of a new variety of refractive index-based optical sensors. This study also supported the hypothesis that the degree of wavefront distortion would also be a function of polymer-solvent solubility parameter match. Selectivity for specific organic compounds could thus potentially be addressed by using target films composed of transparent polymers with different polarities and refractive indices, in patterns with specific geometries. Differential phase-shifting effects in such a 2-D array would be expected to form more complex wavefront distortion patterns related to the chemical nature of the vapor, either as single components or mixtures. Characterization of the wavefront distortion in greater detail using more sophisticated image analysis techniques, such as determination of Zernike coefficients [21], may also offer increased sensitivity and selectivity for such sensors.

Acknowledgments

This work was supported by Eastern Michigan University through awarding of a university Faculty Research Fellowship (FRF) and by the EMU Department of Chemistry through Sellers Research Fund grants.

References

[1] G. Harsanyi, Polymer Films in Sensor Applications–Technology, Materials, Devices and Their Characteristics, Technomic Publishing Co. Inc., 1995, pp. 83–89, 199–206.
[2] J.M. Fini, Microstructure fibres for optical sensing in gases and liquids, Meas. Sci. Technol. 15 (2004) 1120–1128.
[3] I. Shavrin, S. Novotny, A. Shevchenko, H. Ludvigsen, Gas refractometry using a hollow-core photonic bandgap fiber in a Mach–Zehnder-type interferometer, Appl. Phys. Lett. 100 (2012) 051106.
[4] H.J. Patrick, A.D. Kersey, F. Bucholtz, Analysis of the response of long period fibre gratings to external index of refraction, J. Lightw. Technol. 16 (9) (1998) 1606–1612.
[5] Z. Wang, J.R. Heflin, K. Van Cott, R.H. Stolen, S. Ramachandran, S. Ghalmi, Biosensors employing ionic self-assembled multilayers adsorbed on long-period fiber gratings, Sens. Actuators B: Chem. 139 (2009) 618–623.
[6] X. Chen, K. Zhou, L. Zhang, I. Bennion, Dual-peak long-period fiber gratings with enhanced refractive index sensitivity by finely tailored mode dispersion that uses light cladding etching technique, Appl. Opt. 46 (4) (2007) 451–455.
[7] J. Kanka, Design of turn-around-point long-period gratings in a photonic crystal fiber forefractometry of gases, Sens. Actuators B: Chem. 182 (2013) 16–24.
[8] G. Jin, Y.H. Meng, L. Liu, Y. Niu, S. Chen, Q. Cai, T.J. Jiang, Development of biosensor based on imaging ellipsometry and biomedical applications, Thin Solid Films 519 (9) (2011) 2750–2757.
[9] R.S. Moirangthem, Y.-C. Chang, S.-H. Hsu, P.-K. Wei, Surface plasmon resonance ellipsometry based sensor for studying biomolecular interaction, Biosens. Bioelectron. 25 (12) (2010) 2633–2638.
[10] W. Yuan, H.P. Ho, S.Y. Wu, Y.K. Suen, S.K. Kong, Polarization-sensitive surface plasmon enhanced ellipsometry biosensor using the photoelastic modulation technique, Sens.Actuators A: Phys. A151 (1) (2009) 23–28.
[11] M. Mansuripur, The Shack–Hartmann wavefront sensor, Opt. Photonics News (April) (1999) 48–51.
[12] D.R. Neal, J. Copland, D. Neal, Shack–Hartmann wavefront sensor precision and accuracy, Proc. SPIE 4779 (2002) 148–160.
[13] D.R. Neal, W.J. Alford, J.K. Gruetzner, Amplitude and phase beam characterization using a two-dimensional wavefront sensor, Proc. SPIE 2870 (1996) 72–82.
[14] J. Liang, B. Grimm, S. Goelz, J.F. Bille, Objective measurement of the wave aberrations of the human eye with the use of a Hartmann–Shack wavefront sensor, J. Opt. Soc. Am. A Opt. Image Sci. Vis. 11 (1994) 1949–1957.
[15] P.W. Milloni, Adaptive optics in astronomy, Am. J. Phys. 67 (6) (1999) 476–485.
[16] S. Chenais, F. Balembois, P. Georges, R. Gaume, B. Viana, G.P. Aka, D. Vivien, Thermal lensing measurements in diode-pumped Yb-doped materials, Trend. Opt. Photon. 68 (2002) 384–386 (Advanced Solid-State Lasers).
[17] A. Nishimura, K. Akaoka, A. Ohzu, T. Usami, Temporal change of thermal lens effects on highly pumped ytterbium glass by wavefront measurement, J. Nucl. Sci. Technol. 38 (12) (2001) 1043–1047.
[18] D.V. Podanchuk, V.N. Kurashov, A.V. Kovalenko, V.P. Dan'ko, A.V. Yurchenko, Measurement of light-phase distortions in an acousto-optical deflector with Shack–Hartmann wavefront sensor, Proc. SPIE: Int. Soc. Opt. Eng. 3904 (1999) 311–318 (Correlation Optics).
[19] D.M. Snyder, N. Raju, Method and Apparatus for Quantifying the Degree of Fusion of a Layer, United States Patent Application 20050012939, filed by Armstrong World Industries, Inc., Lancaster, Pa, publication date 01/20/05.
[20] J. Brandrup, E.H. Immergut, Grulke (Eds.), Polymer Handbook, 4th ed., Wiley-Interscience, New York, NY, 1999.
[21] J.Y. Wang, D.E. Silva, Wave-front interpretation with Zernike polynomials, Appl. Opt. 19 (1980) 1510–1518.

Biography

Donald M. Snyder received his Ph.D. in Organic Chemistry in 1980 from Purdue University, West Lafayette, Indiana. He was a Project Leader in Corporate Research at Virginia Chemicals, Inc.and then Senior Research Scientist in the Pioneering Research Group at Armstrong World Industries, Inc. before joining the Department of Chemistry at Eastern Michigan University in 1993. His current research focuses on synthesis of specialized polymers for surface functionalization of gold interdigitated electrode arrays for impedance-based sensors and transparent polymers for optical sensors.